

## Hidden nematic fluctuation in the triclinic $(\text{Ca}_{0.85}\text{La}_{0.15})_{10}(\text{Pt}_3\text{As}_8)(\text{Fe}_2\text{As}_2)_5$ superconductor revealed by ultrafast optical spectroscopy

Qi-Yi Wu,<sup>1</sup> Chen Zhang,<sup>1</sup> Ze-Zhong Li,<sup>2</sup> Wen-Shan Hong,<sup>2,3</sup> Hao Liu,<sup>1</sup> Jiao-Jiao Song,<sup>1</sup> Yin-Zou Zhao,<sup>1</sup> Ya-Hua Yuan,<sup>1</sup> Bo Chen,<sup>1</sup> Xue-Qing Ye,<sup>1</sup> Shiliang Li,<sup>2,4</sup> Jun He,<sup>1</sup> H. Y. Liu,<sup>5</sup> Yu-Xia Duan,<sup>1</sup> Hui-Qian Luo,<sup>2,4,\*</sup> and Jian-Qiao Meng<sup>1,†</sup>

<sup>1</sup>*School of Physics, Central South University, Changsha 410083, Hunan, China*

<sup>2</sup>*Beijing National Laboratory for Condensed Matter Physics, Institute of Physics, Chinese Academy of Sciences, Beijing 100190, China*

<sup>3</sup>*International Center for Quantum Materials, School of Physics, Peking University, Beijing 100871, China*

<sup>4</sup>*Songshan Lake Materials Laboratory, Dongguan 523808, China*

<sup>5</sup>*Beijing Academy of Quantum Information Sciences, Beijing 100193, China*



(Received 30 May 2023; accepted 31 October 2023; published 16 November 2023)

We reported the quasiparticle relaxation dynamics of an optimally doped triclinic iron-based superconductor  $(\text{Ca}_{0.85}\text{La}_{0.15})_{10}(\text{Pt}_3\text{As}_8)(\text{Fe}_2\text{As}_2)_5$  with bulk  $T_c = 30$  K using polarized ultrafast optical pump-probe spectroscopy. Our results reveal anisotropic transient reflectivity induced by nematic fluctuations develops below  $T_{\text{nem}} \approx 120$  K and persists in the superconducting states. Measurements under high pump fluence reveal three distinct, coherent phonon modes at frequencies of 1.6, 3.5, and 4.7 THz, corresponding to  $A_{1g}(1)$ ,  $E_g$ , and  $A_{1g}(2)$  modes, respectively. The high-frequency  $A_{1g}(2)$  mode corresponds to the  $c$ -axis polarized vibrations of FeAs planes with a nominal electron-phonon coupling constant  $\lambda_{A_{1g}(2)} = 0.139 \pm 0.02$ . Our results suggest that, at low temperatures, superconducting and nematic states coexist but compete with each other, and it is possible that  $A_{1g}$  phonons are implicated in the formation of Cooper pairs in  $(\text{Ca}_{0.85}\text{La}_{0.15})_{10}(\text{Pt}_3\text{As}_8)(\text{Fe}_2\text{As}_2)_5$ .

DOI: [10.1103/PhysRevB.108.205136](https://doi.org/10.1103/PhysRevB.108.205136)

### I. INTRODUCTION

The discovery of iron-based superconductors (FeSCs) has sparked a new upsurge in the study of high-temperature superconductors (HTSCs) [1]. Although the phase diagram of FeSCs is similar to that of cuprates, the details are different between both families. In particular, the normal state in cuprates is the well-known pseudogap, while its existence in FeSCs remains an open issue [2–4]. Recently, it has been reported that the nematic order is found in the normal state of FeSCs [5–7] and cuprates [8,9], providing a new perspective for understanding the property of pseudogap. Since the nematic order breaks fourfold rotational ( $C_4$ ) symmetry but preserves translational symmetry, it presents as the in-plane anisotropy in various physical quantities. Elucidating the origin of nematic order is considered crucial to understanding the superconductivity in HTSCs. It has been theorized that the spin-driven nematic order and superconductivity with anisotropy gap symmetry ( $s^{+-}$  and  $d$  wave) are a consequence of the magnetic ground state, while orbital-driven nematic order and conventional  $s$ -wave superconductivity are the results of the charging scenario [10–12].

Since the spin and orbital degrees of freedom are strongly coupled to each other, the challenge is how to distinguish experimentally the origin of nematic order [13–16]. Ultrafast spectroscopy offers the possibility to detect and clarify the nematic order in the time domain, based on the distinct relaxation dynamics of various orders [17–20]. Although it is widely accepted that the nematic order may originate

from electrons rather than lattice distortion, recent Raman experiments have shown the presence of significant phonon anomalies in the nematic phase [21,22]. Pump-probe technology can provide some information about the lattice, as the coherent phonon oscillations with Raman activity can be excited by ultrafast lasers [23–26].

In comparison with the other iron-based superconductors, the recently discovered electron-doped  $(\text{Ca}_{1-x}\text{La}_x)_{10}(\text{Pt}_3\text{As}_8)(\text{Fe}_2\text{As}_2)_5$  compound is more similar to the cuprate, whose superconductivity is achieved by the charge doping of FeAs layers rather than the elementary substitution inside the iron layers [27]. Its parent compounds  $\text{Ca}_{10}(\text{Pt}_3\text{As}_8)(\text{Fe}_2\text{As}_2)_5$  (the so-called 10-3-8 system) has a triclinic crystal structure and quasi-two-dimensional (quasi-2D) characters, and each iron arsenide (FeAs) layer has a large separation ( $c_0 = 10.64$  Å) caused by the intercalation of platinum arsenide ( $\text{Pt}_3\text{As}_8$ ) layers and calcium (Ca) planes [Fig. 1(a)] [27,28]. The parent compound shows a structural phase transition at  $T_s = 103$ –110 K, followed by an antiferromagnetic (AFM) transition at  $T_N = 90$ –100 K [29–31]. For optimally doped  $(\text{Ca}_{0.85}\text{La}_{0.15})_{10}(\text{Pt}_3\text{As}_8)(\text{Fe}_2\text{As}_2)_5$  (CaLa-10-3-8), the optical [32] and nuclear magnetic resonance (NMR) measurements [33] indicate that it is a multiple-gap superconductor and has pseudogap behavior.

In this paper, we performed polarized ultrafast optical pump-probe spectroscopy on an optimally electron-doped CaLa-10-3-8 superconductor with bulk  $T_c = 30$  K. Although the signs of the superconducting component along the  $a$  and  $b$  axes are opposite below  $T_c$ , the extracted superconducting gaps using the Rothwarf-Taylor (RT) model are equal, i.e.,  $\Delta_{\text{SC}}^0(0) = \Delta_{\text{SC}}^{90}(0) \approx 11.5 \pm 0.1$  meV. In addition, we observed an anisotropic transient reflectivity induced by

\*Corresponding author: [hqluo@iphy.ac.cn](mailto:hqluo@iphy.ac.cn)

†Corresponding author: [jqmeng@csu.edu.cn](mailto:jqmeng@csu.edu.cn)

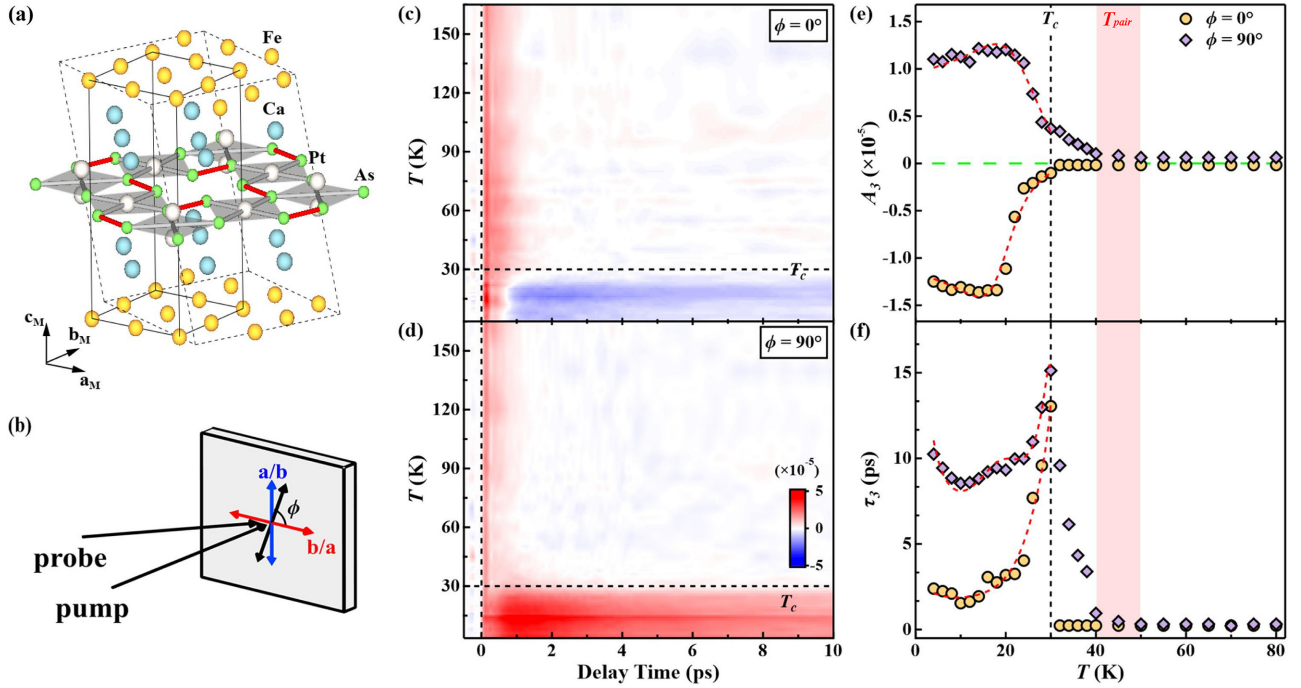


FIG. 1. (a) Crystalline structure of  $(\text{Ca}_{0.85}\text{La}_{0.15})_{10}(\text{Pt}_3\text{As}_8)(\text{Fe}_2\text{As}_2)_5$ . (b) The schematic diagram of the polarized pump-probe spectroscopy. (c) and (d) 2D color map of  $\Delta R(t)/R$  as a function of temperature and delay time at a pump fluence of  $\sim 3.8 \mu\text{J}/\text{cm}^2$ , probed with polarization angles  $\phi = 0^\circ$  and  $\phi = 90^\circ$ , respectively. (e) and (f)  $T$  dependence of amplitudes  $A_3$  and relaxation time  $\tau_3$ , respectively. The red dashed lines are the RT model fitting curves.

the nematic fluctuations that developed from  $T_{\text{nem}} \approx 120$  K and continued below  $T_c$ . Three coherent phonon oscillations  $A_{1g}(1)$ ,  $E_g$ , and  $A_{1g}(2)$  were identified under a high pump fluence. The electron-phonon ( $e$ -ph) coupling constant  $\lambda_{A_{1g}(2)} = 0.139 \pm 0.02$  is estimated for the highest-frequency  $A_{1g}(2)$  mode. Our results suggest that the nematic order is intertwined with superconductivity and coupled with the coherent phonon in CaLa-10-3-8.

## II. EXPERIMENTAL DETAILS

In this study, high-quality single crystals of CaLa-10-3-8 with good cleavage planes (001) were grown using the self-flux method [33]. Ultrafast laser pulses of 800 nm ( $\sim 1.55$  eV) central wavelength, 35 fs pulse width, and 1 MHz repetition rate were used to pump and probe the ultrafast dynamics of the CaLa-10-3-8 sample from 5 to 300 K [24–26]. The polarization of the two beams was varied by rotating the half-wave plate and polarizer in front of the sample; the polarization directions of the probe and pump pulses are maintained perpendicular to each other. The polarization angle is defined as the rotated angle of polarization of probe pulses relative to the horizontal polarization, as shown in Fig. 1(b). Measurements were performed on a freshly cleaved surface under a  $10^{-6}$  mbar vacuum.

## III. RESULTS AND DISCUSSIONS

Figures 1(c) and 1(d) present the 2D pseudocolor  $\Delta R/R$  mapping images with temperature versus delay time along

$\phi = 0^\circ$  and  $\phi = 90^\circ$ , respectively. The relaxation process can be well fitted with the triexponential decays convoluted with a Gaussian laser pulse (see Fig. S2 of Supplemental Material [34]),

$$\frac{R(t)}{R} = \frac{1}{\sqrt{2\pi}w} \exp\left(-\frac{t^2}{2w^2}\right) \otimes \left[ \sum_{i=1}^3 A_i \exp\left(-\frac{t-t_0}{\tau_i}\right) \right] + C, \quad (1)$$

where  $A_i$  and  $\tau_i$  represent the amplitude and relaxation time of the  $i$ th decay process, respectively.  $w$  is the incidence pulse temporal duration, and  $C$  is a constant offset. The initial and briefest relaxation process is always considered as an  $e$ - $e$  scattering process since its extremely short lifetime  $\tau_1$ , typically on the order of a few tens of femtoseconds, which is comparable to the instrument's temporal resolution [24,38].

Figures 1(e) and 1(f) summarize the temperature dependence of the SC response characterized by  $A_3$  and  $\tau_3$  under different polarizations ( $\phi = 0^\circ$  and  $\phi = 90^\circ$ ). For both polarizations, the amplitude  $A_3$  changes suddenly below  $T_c$ . The relaxation time  $\tau_3$  is divergent near  $T_c$ . These features indicate the opening of the superconducting gap, which can be well described by the RT model [24,39–41],

$$A(T) \propto \frac{\varepsilon_I / [\Delta(T) + k_B T / 2]}{1 + \gamma \sqrt{2k_B T} / \pi \Delta(T) e^{-\Delta(T)/k_B T}}, \quad (2)$$

$$\tau \propto \frac{\hbar \omega^2 \ln\{1 / [\varepsilon_I / \alpha \Delta_{\text{SC}}(0)^2 + e^{-\Delta(T)/k_B T}]\}}{12 \Gamma_\omega \Delta(T)^2}, \quad (3)$$

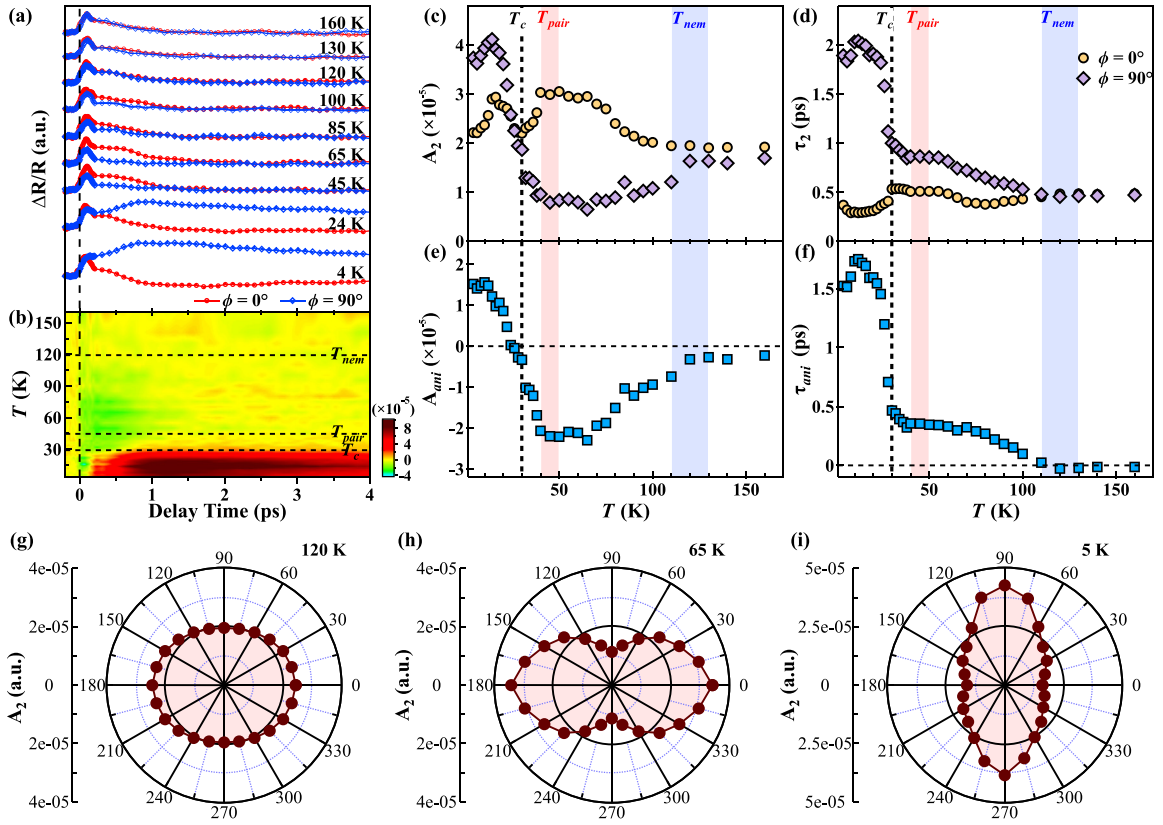


FIG. 2. (a)  $\Delta R(t)/R$  as a function of delay time probed with  $\phi = 0^\circ$  and  $\phi = 90^\circ$  at selected temperatures. (b) The intensity difference between  $\phi = 90^\circ$  and  $\phi = 0^\circ$  [ $(\Delta R/R)_{90} - (\Delta R/R)_0$ ]. (c) and (d)  $T$  dependence of amplitudes  $A_2$  and relaxation time  $\tau_2$ , respectively. (e) and (f) Difference of amplitude  $A_2$  and relaxation time  $\tau_2$  between two polarizations,  $A_{ani} = A_{2,90} - A_{2,0}$ ,  $\tau_{ani} = \tau_{2,90} - \tau_{2,0}$ . (g)–(i) Polarization dependence of amplitude  $A_2$  at selected temperatures.

where  $\varepsilon_l$  is the absorbed laser energy density per unit cell.  $\gamma$ ,  $\omega$ ,  $\alpha$ , and  $\Gamma_\omega$  are the fitting parameters. Figures 1(e) and 1(f) present a good fit to the experimental data below  $T_c$ , giving a zero-temperature gap of  $\Delta_{SC}(0) \approx 11.5 \pm 0.1$  meV for both polarizations, with a typical Bardeen-Cooper-Schrieffer (BCS) form of the temperature dependence gap  $\Delta(T) = \Delta_{SC}(0)[1 - (T/T_c)]^{1/2}$  [42,43]. The SC gap obtained in our study is consistent with the larger SC gap obtained by optical conductivity measurements ( $\approx 14.2$  meV) [32]. It is worth emphasizing that, despite the observable anisotropy in  $A_3$  as the polarization direction is rotated from  $\phi = 0^\circ$  to  $\phi = 90^\circ$ , it does not inherently provide direct insights into the symmetry of the superconducting gap structure. This anisotropy may arise from multiple factors, including the anisotropy of probe transition matrix elements or the anisotropy of the spectral weight transfer in the real part of optical conductivity [35,44]. In addition,  $A_{3,90}$  and  $\tau_{3,90}$  fluctuate above  $T_c$  and vanish around 45 K. This temperature is consistent with the characteristic temperature  $T_{pair} = 45$  K obtained from recent inelastic neutron scattering (INS), Nernst effect, and nuclear magnetic resonance (NMR) experiments, which is related to the SC fluctuation [33]. Thus,  $T_{pair}$  could mark the emergence of preformed Cooper pairs [45].

Figure 2(a) compares the transient reflectivity along  $\phi = 0^\circ$  and  $\phi = 90^\circ$  at different temperatures. At high temperatures, the transient reflectivity along both polarizations is the same. As the temperature decreases,  $\Delta R/R$  of the two

polarizations begins to differ. Initially, the difference appears below  $\sim 2$  ps, and as the temperature drops further, the relative intensities of the two flip and the time range of the difference expands. The difference plot  $(\Delta R/R)_{ani} = (\Delta R/R)_{90} - (\Delta R/R)_0$  is shown in Fig. 2(b) and reveals a clear polarization anisotropy. In addition to the significant positive  $(\Delta R/R)_{ani}$  in the superconducting state, a negative  $(\Delta R/R)_{ani}$ , contributed by a second relaxation process, occurs below  $\sim 120$  K with a lifetime within 2 ps, which is suppressed below  $T_{pair}$  [the green region in Fig. 2(b)]. Figures 2(c) and 2(d) summarized the amplitudes and relaxation times of the second relaxation process along both polarizations. At high temperatures, the amplitude and relaxation time along both polarizations are almost equal and independent of the temperature. As the temperature cools below  $\approx 120$  K, both amplitudes and relaxation times along different polarizations show an opposite tendency with decreasing temperature, which implies a break in symmetry. This anisotropy is more clearly in  $A_{ani} = A_{2,0} - A_{2,90}$  and  $\tau_{ani} = \tau_{2,0} - \tau_{2,90}$  [Figs. 2(e) and 2(f)]. Below  $\approx 120$  K,  $A_{ani}$  shows an apparent reduction, and  $\tau_{ani}$  increases with decreasing temperature. Therefore, it is reasonable to argue that here in  $(Ca_{0.85}La_{0.15})_{10}(Pt_3As_8)(Fe_2As_2)_5$  the nematic fluctuations occur with an onset temperature at  $T_{nem} \approx 120$  K.

To further elucidate the broken symmetry, we performed a polarized experiment at selected temperatures and extracted the angular dependence of  $A_2$  by using Eq. (1), as shown in Figs. 2(g)–2(i). At a temperature of 120 K, approximately

$T_{\text{nem}}$ ,  $A_2$  is almost isotropic [Fig. 2(g)]. At 65 K, well below  $T_{\text{nem}}$ ,  $A_2$  at  $\phi = 0^\circ$  shows a maximum, while that at  $\phi = 90^\circ$  shows a minimum [Fig. 2(h)].  $A_2$  shows twofold symmetry, clearly demonstrating the breaking of fourfold rotational symmetry. This transient anisotropy is also observed in other FeSCs [17–20,46] and attributed to the nematic fluctuations contributed by the vestigial phase from rotation-symmetry-broken electronic states. In our study, one possible explanation is the orbital scenario, which accounts for the qualitative difference between  $\phi = 0^\circ$  and  $\phi = 90^\circ$ . In FeSCs, the optical response to 1.55 eV photons is primarily attributed to Fe 3d orbitals [47,48]. Similar to other FeSCs, experimental and theoretical calculations indicate that the density of states near the Fermi energy in the 10-3-8 system mainly comes from Fe 3d orbitals [49–51]. Based on the band structures near the Fermi energy [51], the optical response to 1.55 eV photons in the 10-3-8 system may also primarily result from the Fe 3d-Fe 3d transition. With linearly polarized light, the probe pulses polarized along the  $a$  and  $b$  axes are sensitive to  $d_{xz}$  and  $d_{yz}$  orbits, respectively [52]. In the presence of nematic fluctuations with orbital origins, the splitting between the originally degenerate  $d_{xz}$  and  $d_{yz}$  orbits results in varying populations in these two orbits, thereby causing the observed reflectivity anisotropy [7,18]. Additionally, a spin-based nematic order is also a viable explanation. Recent NMR experiments have indicated a rapid increase in the spin-lattice relaxation of CaLa-10-3-8 above 150 K, suggesting a symmetry breaking in the spin degree of freedom [33]. Further investigations, including probing the ellipticity of the probe beam, are necessary to confirm whether the nematic state is driven by spin fluctuations in the future.

Moreover,  $A_{\text{ani}}$  and  $\tau_{\text{ani}}$  change simultaneously around  $T_{\text{pair}} = 45$  K. Near  $T_c$ , the relative amplitudes of  $A_{2,0}$  and  $A_{2,90}$  are reversed [Fig. 2(c)], resulting in a change in the sign of  $A_{\text{ani}}$  [Fig. 2(e)]. As shown in Fig. 2(i), at 5 K, well below  $T_c$ ,  $A_2$  reaches a maximum at  $\phi = 90^\circ$  and a minimum at  $\phi = 0^\circ$ . That is, the superconducting transition results in a  $90^\circ$  rotation of  $A_2$ 's long axis, signifying a strong coupling and competition between the nematic state and superconductivity. This also suggests that  $A_2$  may contain indirect information about the superconducting order symmetry. When  $T_{\text{nem}} > T > T_c$ , the relaxation processes are primarily governed by nematic fluctuations. After pump pulses weaken the nematic fluctuations, it will rapidly recover to equilibrium. Below  $T_c$ , relaxation processes combine nematic and superconducting responses. Pump pulses not only weaken nematic fluctuations but also suppress superconductivity. The nonequilibrium nematic order will not recover towards its equilibrium, but towards a time-dependent quasiequilibrium with the form of superconducting order parameters. Thus, below  $T_c$ , the nematic fluctuations are enhanced by mutual repulsion and are also affected by superconductivity [46]. According to this picture, the rotation of the long axis below  $T_c$  can be naturally interpreted as follows: When temperature crosses  $T_c$ , the nematic signals along  $\phi = 90^\circ$  will be enhanced by a positive superconducting response, while the nematic signals along  $\phi = 0^\circ$  will be reduced by a negative superconducting signal.

In addition to the quasiparticle relaxation dynamics under low fluence, we also focus on the behaviors of a coherent phonon which is excited by the high fluence laser pulses. Ap-

parent oscillations appear in  $\Delta R(t)/R$ , as shown in Fig. 3(a). The oscillatory components are obtained by performing the fast Fourier transform (FFT) on the oscillation extracted by subtracting the exponential decay from the  $\Delta R(t)/R$ . The inset in Fig. 3(a) presents three terahertz modes with frequencies of  $\omega_1/2\pi \sim 1.6$  THz (i.e., 6.6 meV or  $53.4 \text{ cm}^{-1}$ ),  $\omega_2/2\pi \sim 3.5$  THz (i.e., 14.5 meV or  $116.7 \text{ cm}^{-1}$ ), and  $\omega_3/2\pi \sim 4.7$  THz (i.e., 19.4 meV or  $156.8 \text{ cm}^{-1}$ ). To date, Raman spectroscopy studies or phonon calculations of the Ca10-3-8 materials are lacking. However, other iron-based superconductor families with FeAs layers show Raman-active phonons near these energies. Both the lowest component,  $\omega_1$ , and the primary component,  $\omega_3$ , are  $A_{1g}$  modes, denoted as  $A_{1g}(1)$  and  $A_{1g}(2)$  [24,53], respectively. These modes correspond to  $c$ -axis polarized vibrations of the FeAs layers [53]. Considering the frequency of the  $\omega_2$  phonon and its polarization dependence [Fig. 3(b)], we classify it as an  $E_g$  mode, associated with the in-plane asymmetry of the FeAs layers [36,54–56].

The ultrafast spectroscopy measurements on other FeSCs revealed that the  $e$ -ph coupling constant  $\lambda_{A_{1g}}$  is proportional to  $T_c$  [37], suggesting that the  $A_{1g}$  mode plays an essential role in forming Cooper pairs [37]. Our estimation of  $\lambda_{A_{1g}(2)}$  for CaLa-10-3-8 yielded a value of  $0.139 \pm 0.02$  (detailed calculations can be found in the Supplemental Material [34]), falling within the range described in Ref. [37]. This indicates a commonality in the superconducting mechanism between CaLa-10-3-8 and other FeSCs, although the doping scenario of CaLa-10-3-8 is more similar to the cuprate in previous work [27].

Figure 3(c) presents the 2D pseudocolor mapping image of  $\Delta R(t)/R$  as a function of temperatures and delay time. The oscillation survives up to room temperature and can be fitted by the following expression [black curves in Fig. 3(d)],

$$\left( \frac{\Delta R}{R} \right)_{\text{osc}} = \sum_{j=1}^3 A_j e^{-\Gamma_j t} \sin(\omega_j t + \phi_j), \quad (4)$$

where  $A_j$ ,  $\Gamma_j$ ,  $\omega_j$ , and  $\phi_j$  are the  $j$ th oscillatory signal amplitude, damping rate, frequency, and initial phase, respectively. The extracted temperature evolutions of frequencies and damping rates are plotted in Figs. 3(e) and 3(f). The temperature dependence of  $E_g$ ,  $A_{1g}(1)$ , and  $A_{1g}(2)$  phonons at high temperatures aligns well with anharmonic effects [24,57,58]. However, this model fails to explain the behavior of  $A_{1g}(1)$  and  $A_{1g}(2)$  phonons at low temperatures. Below  $T_{\text{nem}}$ ,  $\omega_3$  deviates from the anharmonic effect curve, indicating possible coupling between the  $A_{1g}(2)$  phonon and nematic order [diamond in Fig. 3(e)]. The temperature-dependent damping rate  $\Gamma_3$  shows minimal variation, making it challenging to definitively confirm any deviation from the anharmonic effects in the current results. Additionally, phonon softening in  $\omega_1$  and divergence in  $\Gamma_1$  were simultaneously observed around  $T_c$  [open squares in Figs. 3(e) and 3(f)], suggesting a potential connection between the  $A_{1g}(1)$  mode and the opening of the superconducting gap  $\Delta_{\text{SC}}$  [42].

#### IV. CONCLUSIONS

In conclusion, we have used polarized ultrafast optical spectroscopy to investigate the quasiparticle dynamics

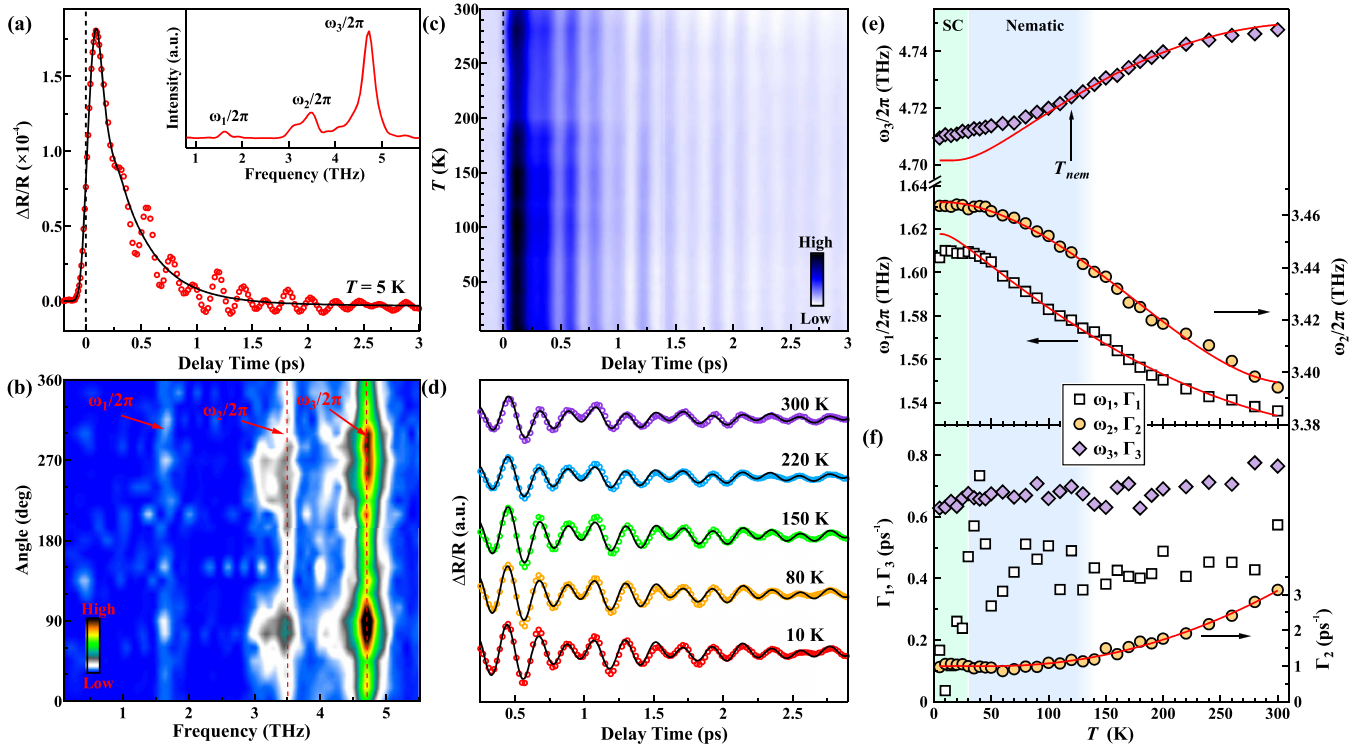


FIG. 3. (a) Typical  $\Delta R(t)/R$  curves at a pump fluence of  $\sim 122.8 \mu\text{J}/\text{cm}^2$  along  $\phi = 90^\circ$ , composed of quasiparticle relaxation (black solid line) and coherent optical phonon vibration. Inset: FFT results showing three phonon modes with frequency of 1.6, 3.5, and 4.7 THz. (b) 2D map of FFT results as a function of polar angle and frequency at 5 K. (c) 2D color map of  $\Delta R(t)/R$  as a function of temperature and delay time. (d) Phonon oscillations extracted at five temperatures. The black lines are Eq. (4) fits. (e) and (f) The derived frequency and damping rate, respectively, as a function of temperature. The red solid lines are fitted curves using the anharmonic phonon model.

and coherent phonons of  $(\text{Ca}_{0.85}\text{La}_{0.15})_{10}(\text{Pt}_3\text{As}_8)(\text{Fe}_2\text{As}_2)_5$  with  $T_c = 30$  K. An anisotropy transient reflectivity induced by the nematic fluctuations emerges below  $T_{\text{nem}} \approx 120$  K, coexisting and competing with the superconductivity [ $\Delta_{\text{SC}}(0) \approx 11.5 \pm 0.1$  meV]. Three coherent phonons were observed at 1.6 [ $A_{1g}(1)$  mode], 3.5 ( $E_g$  mode), and 4.7 THz [ $A_{1g}(2)$  mode]. The high-frequency  $A_{1g}(2)$  mode with  $\lambda_{A_{1g}(2)} = 0.139 \pm 0.02$  deviates from the curve accounting for phonon anharmonic effects at low temperatures. Our results provide critical information for understanding the relationship between the superconductivity and the nematic state in quasi-2D FeSCs and prove the  $A_{1g}$  phonons are closely related to the superconductivity and nematic ordering in  $(\text{Ca}_{0.85}\text{La}_{0.15})_{10}(\text{Pt}_3\text{As}_8)(\text{Fe}_2\text{As}_2)_5$ .

## ACKNOWLEDGMENTS

This work was supported by the National Natural Science Foundation of China (Grants No. 92265101, No. 12074436, No. 11822411, and No. 11961160699), and the National Key Research and Development Program of China (Grants No. 2022YFA1604204 and No. 2018YFA0704200). J.Q.M. would like to acknowledge support from the Science and Technology Innovation Program of Hunan Province (2022RC3068). H.Q.L. was supported by the Youth Innovation Promotion Association of CAS (Grant No. Y202001). W.S.H. was supported by the Postdoctoral Innovative Talent program (Grant No. BX2021018), and the China Postdoctoral Science Foundation (Grant No. 2021M700250).

[1] Y. Kamihara, T. Watanabe, M. Hirano, and H. Hosono, *J. Am. Chem. Soc.* **130**, 3296 (2008).  
 [2] M. Hashimoto, I. M. Vishik, R. H. He, T. P. Devereaux, and Z. X. Shen, *Nat. Phys.* **10**, 483 (2014).  
 [3] D. C. Johnston, *Adv. Phys.* **59**, 803 (2010).  
 [4] J. Paglione and R. L. Greene, *Nat. Phys.* **6**, 645 (2010).  
 [5] H. H. Kuo, J. H. Chu, J. C. Palmstrom, S. A. Kivelson, and I. R. Fisher, *Science* **352**, 958 (2016).  
 [6] A. Dusza, A. Lucarelli, F. Pfuner, J. H. Chu, I. R. Fisher, and L. Degiorgi, *Europhys. Lett.* **93**, 37002 (2011).  
 [7] M. Yi, D. H. Lu, J. H. Chu, J. G. Analytis, A. P. Sorini, A. F. Kemper, B. Moritz, S. K. Mo, R. G. Moore, M. Hashimoto,

W. S. Lee, Z. Hussain, T. P. Devereaux, I. R. Fisher, and Z. X. Shen, *Proc. Natl. Acad. Sci. USA* **108**, 6878 (2011).  
 [8] V. Hinkov, D. Haug, B. Fauqu, P. Bourges, Y. Sidis, A. Ivanov, C. Bernhard, C. T. Lin, and B. Keimer, *Science* **319**, 597 (2008).  
 [9] J. Wu, A. T. Bollinger, X. He, and I. Bozovic, *Nature (London)* **547**, 432 (2017).  
 [10] R. M. Fernandes, A. V. Chubukov, and J. Schmalian, *Nat. Phys.* **10**, 97 (2014).  
 [11] H. Yamase and R. Zeyher, *Phys. Rev. B* **88**, 180502(R) (2013).  
 [12] T. Agatsuma and H. Yamase, *Phys. Rev. B* **94**, 214505 (2016).

- [13] M. D. Watson, T. K. Kim, A. A. Haghighirad, N. R. Davies, A. McCollam, A. Narayanan, S. F. Blake, Y. L. Chen, S. Ghannadzadeh, A. J. Schofield, M. Hoesch, C. Meingast, T. Wolf, and A. I. Coldea, *Phys. Rev. B* **91**, 155106 (2015).
- [14] S. H. Baek, D. V. Efremov, J. M. Ok, J. S. Kim, J. van den Brink, and B. Buchner, *Nat. Mater.* **14**, 210 (2015).
- [15] Q. Zhang, R. M. Fernandes, J. Lamsal, J. Yan, S. Chi, G. S. Tucker, D. K. Pratt, J. W. Lynn, R. W. McCallum, P. C. Canfield, T. A. Lograsso, A. I. Goldman, D. Vaknin, and R. J. McQueeney, *Phys. Rev. Lett.* **114**, 057001 (2015).
- [16] M. G. Kim, R. M. Fernandes, A. Kreyssig, J. W. Kim, A. Thaler, S. L. Budko, P. C. Canfield, R. J. McQueeney, J. Schmalian, and A. I. Goldman, *Phys. Rev. B* **83**, 134522 (2011).
- [17] C. W. Luo, P. C. Cheng, S. H. Wang, J. C. Chiang, J. Y. Lin, K. H. Wu, J. Y. Juang, D. A. Chareev, O. S. Volkova, and A. N. Vasiliev, *npj Quantum Mater.* **2**, 32 (2017).
- [18] S. H. Liu, C. F. Zhang, Q. Deng, H. H. Wen, J. X. Li, E. E. M. Chia, X. Y. Wang, and M. Xiao, *Phys. Rev. B* **97**, 020505(R) (2018).
- [19] A. Patz, T. Li, S. Ran, R. M. Fernandes, J. Schmalian, S. L. Bud'ko, P. C. Canfield, I. E. Perakis, and J. Wang, *Nat. Commun.* **5**, 3229 (2014).
- [20] L. Stojchevska, T. Mertelj, J.-H. Chu, Ian R. Fisher, and D. Mihailovic, *Phys. Rev. B* **86**, 024519 (2012).
- [21] V. K. Thorsmølle, M. Khodas, Z. P. Yin, C. L. Zhang, S. V. Carr, P. C. Dai, and G. Blumberg, *Phys. Rev. B* **93**, 054515 (2016).
- [22] P. Massat, D. Farina, I. Paul, S. Karlsson, P. Strobel, P. Toulemonde, M. A. Measson, M. Cazayous, A. Sacuto, S. Kasahara, T. Shibauchi, Y. Matsuda, and Y. Gallais, *Proc. Natl. Acad. Sci. USA* **113**, 9177 (2016).
- [23] W. Albrecht, T. Kruse, and H. Kurz, *Phys. Rev. Lett.* **69**, 1451 (1992).
- [24] C. Zhang, Q. Y. Wu, W. S. Hong, H. Liu, S. X. Zhu, J. J. Song, Y. Z. Zhao, F. Y. Wu, Z. T. Liu, S. Y. Liu, Y. H. Yuan, H. Huang, J. He, S. L. Li, H. Y. Liu, Y. X. Duan, H. Q. Luo, and J. Q. Meng, *Sci. China: Phys. Mech. Astron.* **65**, 237411 (2022).
- [25] S. X. Zhu, C. Zhang, Q. Y. Wu, X. F. Tang, H. Liu, Z. T. Liu, Y. Luo, J. J. Song, F. Y. Wu, Y. Z. Zhao, S. Y. Liu, T. Le, X. Lu, H. Ma, K. H. Liu, Y. H. Yuan, H. Huang, J. He, H. Y. Liu, Y. X. Duan *et al.*, *Phys. Rev. B* **103**, 115108 (2021).
- [26] S. Y. Liu, S. X. Zhu, Q. Y. Wu, C. Zhang, P. B. Song, Y. G. Shi, H. Liu, Z. T. Liu, J. J. Song, F. Y. Wu, Y. Z. Zhao, X. F. Tang, Y. H. Yuan, H. Huang, J. He, H. Y. Liu, Y. X. Duan, and J. Q. Meng, *Results Phys.* **30**, 104816 (2021).
- [27] T. Stürzer, G. Derondeau, and D. Johrendt, *Phys. Rev. B* **86**, 060516(R) (2012).
- [28] N. Ni, J. M. Allred, B. C. Chan, and R. J. Cava, *Proc. Natl. Acad. Sci. USA* **108**, E1019 (2011).
- [29] N. Ni, W. E. Straszheim, D. J. Williams, M. A. Tanatar, R. Prozorov, E. D. Bauer, F. Ronning, J. D. Thompson, and R. J. Cava, *Phys. Rev. B* **87**, 060507(R) (2013).
- [30] P. W. Gao, L. L. Sun, N. Ni, J. Guo, Q. Wu, C. Zhang, D. C. Gu, K. Yang, A. G. Li, S. Jiang, R. J. Cava, and Z. X. Zhao, *Adv. Mater.* **26**, 2346 (2014).
- [31] A. Sapkota, G. S. Tucker, M. Ramazanoglu, W. Tian, N. Ni, R. J. Cava, R. J. McQueeney, A. I. Goldman, and A. Kreyssig, *Phys. Rev. B* **90**, 100504(R) (2014).
- [32] Y. I. Seo, W. J. Choi, S. I. Kimura, Y. Bang, and Y. S. Kwon, *Phys. Rev. B* **95**, 094510 (2017).
- [33] Z. Z. Li, W. S. Hong, H. L. Zhou, X. Y. Ma, U. Stuhr, K. Y. Zeng, L. Ma, Y. Xiang, H. Yang, H. H. Wen, J. P. Hu, S. L. Li, and H. Q. Luo (unpublished).
- [34] See Supplemental Material at <http://link.aps.org/supplemental/10.1103/PhysRevB.108.205136> for additional experimental results and a supporting data analysis, which includes Refs. [35–37].
- [35] D. Dvorsek, V. V. Kabanov, J. Demsar, S. M. Kazakov, J. Karpinski, and D. Mihailovic, *Phys. Rev. B* **66**, 020510(R) (2002).
- [36] A. Baum, Ying Li, M. Tomić, N. Lazarević, D. Jost, F. Löffler, B. Muschler, T. Böhm, J. H. Chu, I. R. Fisher, R. Valentí, I. I. Mazin, and R. Hackl, *Phys. Rev. B* **98**, 075113 (2018).
- [37] Q. Wu, H. X. Zhou, Y. L. Wu, L. L. Hu, S. L. Ni, Y. C. Tian, F. Sun, F. Zhou, X. L. Dong, Z. X. Zhao, and J. M. Zhao, *Chin. Phys. Lett.* **37**, 097802 (2020).
- [38] K. H. Lin, K. J. Wang, C. C. Chang, Y. C. Wen, D. H. Tsai, Y. R. Wu, Y. T. Hsieh, M. J. Wang, B. Lv, P. C.-W. Chu, and M. K. Wu, *Phys. Rev. B* **90**, 174502 (2014).
- [39] A. Rothwarf and B. N. Taylor, *Phys. Rev. Lett.* **19**, 27 (1967).
- [40] Y. H. Liu, Y. Toda, K. Shimatake, N. Momono, M. Oda, and M. Ido, *Phys. Rev. Lett.* **101**, 137003 (2008).
- [41] E. E. M. Chia, D. Talbayev, J. X. Zhu, H. Q. Yuan, T. Park, J. D. Thompson, C. Panagopoulos, G. F. Chen, J. L. Luo, N. L. Wang, and A. J. Taylor, *Phys. Rev. Lett.* **104**, 027003 (2010).
- [42] J. Qi, T. Durakiewicz, S. A. Trugman, J. X. Zhu, P. S. Riseborough, R. Baumbach, E. D. Bauer, K. Gofryk, J. Q. Meng, J. J. Joyce, A. J. Taylor, and R. P. Prasankumar, *Phys. Rev. Lett.* **111**, 057402 (2013).
- [43] Y. Z. Zhao, Q. Y. Wu, C. Zhang, B. Chen, W. Xia, J. J. Song, Y. H. Yuan, H. Liu, F. Y. Wu, X. Q. Ye, H. Y. Zhang, H. Huang, H. Y. Liu, Y. X. Duan, Y. F. Guo, J. He, and J. Q. Meng, *Phys. Rev. B* **108**, 075115 (2023).
- [44] G. P. Segre, N. Gedik, J. Orenstein, D. A. Bonn, R. Liang, and W. N. Hardy, *Phys. Rev. Lett.* **88**, 137001 (2002).
- [45] M. A. Surmach, F. Brückner, S. Kamusella, R. Sarkar, P. Y. Portnichenko, J. T. Park, G. Ghambashidze, H. Luetkens, P. K. Biswas, W. J. Choi, Y. I. Seo, Y. S. Kwon, H. H. Klauss, and D. S. Inosov, *Phys. Rev. B* **91**, 104515 (2015).
- [46] E. Thewalt, I. M. Hayes, J. P. Hinton, A. Little, S. Patankar, L. Wu, T. Helm, C. V. Stan, N. Tamura, J. G. Analytis, and J. Orenstein, *Phys. Rev. Lett.* **121**, 027001 (2018).
- [47] A. V. Boris, N. N. Kovaleva, S. S. A. Seo, J. S. Kim, P. Popovich, Y. Matiks, R. K. Kremer, and B. Keimer, *Phys. Rev. Lett.* **102**, 027001 (2009).
- [48] A. Charnukha, P. Popovich, Y. Matiks, D. L. Sun, C. T. Lin, A. N. Yaresko, B. Keimer, and A. V. Boris, *Nat. Commun.* **2**, 219 (2010).
- [49] M. Neupane, C. Liu, S. Y. Xu, Y. J. Wang, N. Ni, J. M. Allred, L. A. Wray, N. Alidoust, Hsin Lin, R. S. Markiewicz, A. Bansil, R. J. Cava, and M. Z. Hasan, *Phys. Rev. B* **85**, 094510 (2012).
- [50] S. Thirupathaiah, T. Stürzer, V. B. Zabolotnyy, D. Johrendt, B. Büchner, and S. V. Borisenko, *Phys. Rev. B* **88**, 140505(R) (2013).
- [51] T. Berljin, *Phys. Rev. B* **89**, 104511 (2014).
- [52] T. Shimojima, K. Ishizaka, Y. Ishida, N. Katayama, K. Ohgushi, T. Kiss, M. Okawa, T. Togashi, X. Y. Wang, C. T. Chen, S. Watanabe, R. Kadota, T. Oguchi, A. Chainani, and S. Shin, *Phys. Rev. Lett.* **104**, 057002 (2010).

- [53] K. Y. Choi, D. Wulferding, P. Lemmens, N. Ni, S. L. Bud'ko, and P. C. Canfield, *Phys. Rev. B* **78**, 212503 (2008).
- [54] R. A. Jishi and H. M. Alyahyaei, *Adv. Condens. Matter Phys.* **2010**, 804343 (2010).
- [55] R. Merlin, *Solid State Commun.* **102**, 207 (1997).
- [56] A. P. Litvinchuk, B. Lv, and C. W. Chu, *Phys. Rev. B* **84**, 092504 (2011).
- [57] J. Menéndez and M. Cardona, *Phys. Rev. B* **29**, 2051 (1984).
- [58] S. Y. Zhang, J. Q. Guan, X. Jia, B. Liu, W. H. Wang, F. S. Li, L. L. Wang, X. C. Ma, Q. K. Xue, J. D. Zhang, E. W. Plummer, X. T. Zhu, and J. D. Guo, *Phys. Rev. B* **94**, 081116(R) (2016).